Linear and nonlinear light scattering near the phase transition in KH_2PO_4

I. Drevenšek, M. Zgonik,* M. Čopič, and R. Blinc
Jožef Stefan Institute, University of Ljubljana, Slovenia

A. Fuith, W. Schranz, M. Fally, and H. Warhanek
Institute of Experimental Physics, Vienna University, Vienna, Austria
(Received 16 August 1993)

The angular and temperature dependence of the linear light scattering and the temperature dependence of the second-harmonic nonlinear light scattering were studied in two different samples of KH_2PO_4 (KDP) crystal: one from a zone close to the seed and another from a zone far from the seed. The angular dependence of the intensity of the linearly scattered light from the sample from the zone close to the seed shows a strong peak for the near $Z(YX)Y$ scattering. This scattering originates from growth bands parallel to the $(0\bar{1}1)$ lattice planes in the pyramidal growth sector. The temperature dependence of the magnitude of this peak shows a considerable increase in the vicinity of the phase transition from the paraelectric to ferroelectric phase. Such an increase in the linear light scattering was not observed in the sample from the zone far from the seed. The anomalies related to the growth bands parallel to the (010) lattice planes in the prismatic growth sector were investigated also by second-harmonic light scattering. Here again a considerable increase in the intensity of the frequency-doubled scattered light was observed in the vicinity of the phase-transition temperature. The results of the light-scattering experiments are compared with an x-ray topographic study of the lattice defects.

I. INTRODUCTION

The origin of the quasielastic central peaks, occurring in addition to the soft mode in the Brillouin scattering spectra in a number of structural phase transitions, has been for some time the subject of intensive investigations. A particularly intense central peak which nearly disappears after annealing was observed in KH_2PO_4 (KDP).[1-5] Annealing, however, does not affect the occurrence of small dynamic clusters seen in these systems by NMR and EPR.[6]

The prominent increase of the strength of the central peak in KDP is connected with the increase in the strain decoration of lattice defects on approaching the transition temperature T_c, where the harmonic part of the critical elastic constant C_{66}, related to the soft acoustic mode, vanishes. Mechanisms corresponding to different types of lattice defects have been considered, such as stacking faults and dislocations, or point defects.[7-9] Despite various considerations, a quantitative understanding of the central peak has not yet been obtained due to the lack of information on the nature of the defects in the samples that were used in the experimental investigations.[10]

In order to check more quantitatively the proposed mechanisms we decided to investigate the linear and nonlinear light scattering from different KDP samples, with a known concentration of the impurities and with well characterized lattice defects. In our case the intensity of the linear and nonlinear second-harmonic light scattering without spectral resolution was measured. The nonlinear light scattering was measured in a geometry where no second-harmonic generation is allowed in an ideal crystal neither above nor below the paraelectric-ferroelectric transition temperature T_c. After light-scattering measurements the structure of lattice defects in the samples was determined by x-ray topographing. The concentration of the impurities was determined by light emission spectroscopy.

II. EXPERIMENT

Large crystals of KDP were grown from {011} seed plates by controlled evaporation of the aqueous solution at a growth temperature of 30 ± 0.003 °C. The details of the growth method and growth vessel are described elsewhere.[11] The growth solution has been purified by sixfold recrystallizations and the amount of impurities measured by light emission spectroscopy. After this procedure the concentration of the impurities in the final mother liqueur was less than 10 ppm, with Na^+ ions (≈ 5 ppm) being the main impurity.

It is known that in KDP crystals grown from {011} seed plates a majority of dislocations grow in a direction perpendicular to the seed plate, so that they "grow out" of the crystal and the part of the crystal far from the seed is rather free of dislocations and other defects.[12] This feature is clearly visible in Fig. 1(b) which shows a topograph of one of our crystals with a lot of Rb impurities ($\approx 15\,000$ ppm) being added to obtain high contrast of the topograph. In purified crystals, which has been used for the light-scattering investigations, the density of the lattice defects and their contrast on the topographs are strongly decreased.

For light-scattering experiments one sample with dimensions $9\times6\times5$ mm^3 from the zone close to the seed ($S1$) and another one sample with dimensions $8\times6\times6$ mm^3 from the zone far from the seed ($S2$) were cut from

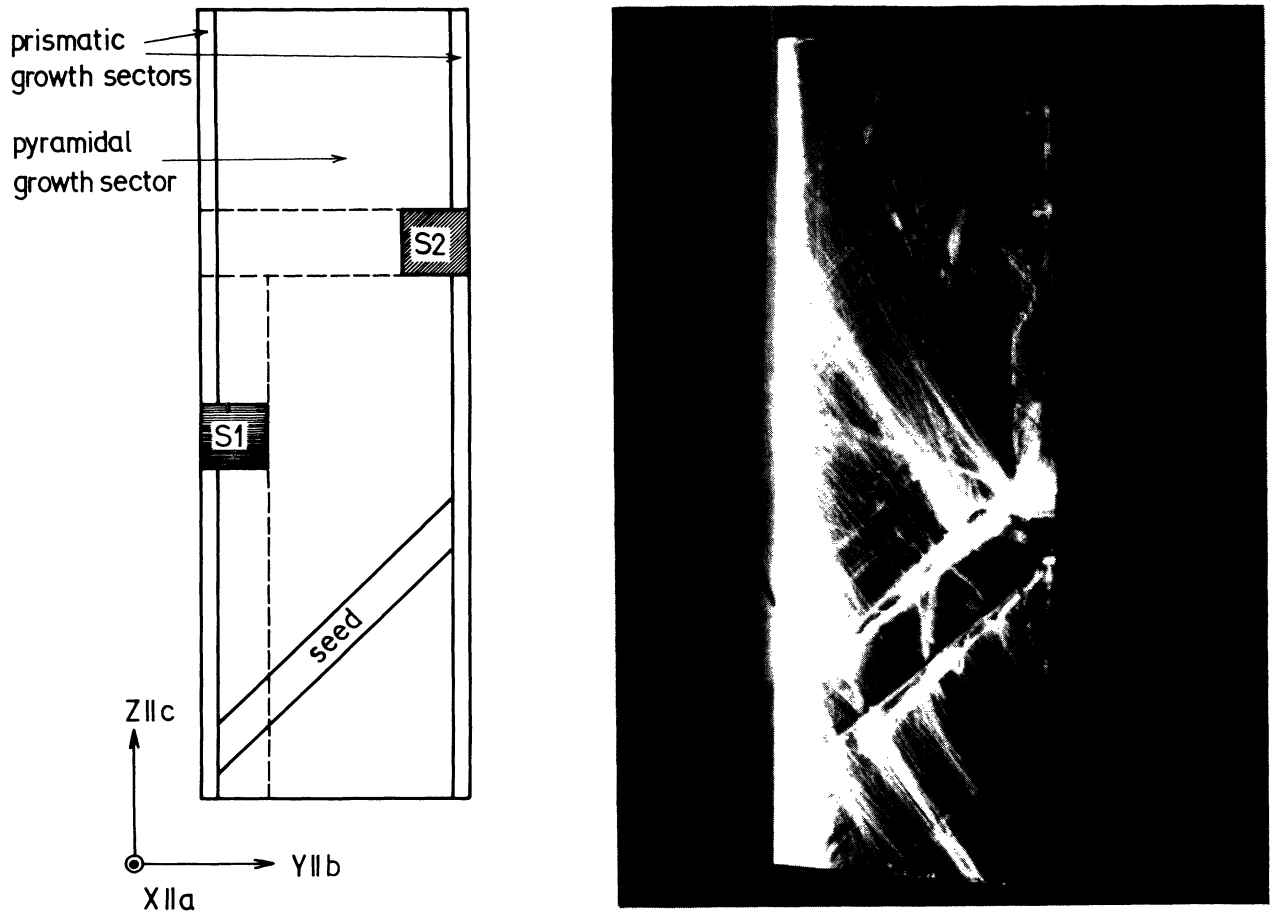

FIG. 1. (a) Schematic drawing of an X cut of the crystal, showing the regions which were sawed for the samples $S1$ and $S2$. (b) X-ray topograph of an X cut of the crystal with high density (15 000 ppm) of impurities.

one of such large purified crystals. This way the samples had the same purity and growth history and differed only in the properties related to the vicinity of the seed plate. Both samples included some part of the pyramidal and some part of the prismatic growth sector of the crystal. A boundary between the growth sectors in the samples was determined from surface changes obtained by etching of the samples in the water-alcohol (1:1) mixture. After this the samples were polished to optical quality. The regions of the original crystal that were used as the samples are illustrated in Fig. 1(a). The orientation of the reference coordinate system is chosen in accordance to Fig. 1(b).

A. Linear scattering

The sample was mounted in the center of a rotation stage, which allowed rotating the detector around the sample. As a light source for the investigations of linear light scattering a cw Ar-ion laser operating at $\lambda = 514.5$ nm with 100 mW output power was used. The incident laser beam propagated through the sample along the Z ($\|c$) crystallographic axis, which was previously determined by observation of the birefringence (the center of conoscopic cross). The beam was linearly polarized along the Y ($\|b$) axis and focused onto the sample by a lens with a focal length of 100 mm. The scattered radiation was collected by another lens ($f = 100$ mm) and focused onto a photomultiplier. The polarization of the detected scattered light was determined by a polarizer mounted in front of the photomultiplier.

The angular dependence of the intensity of the scattered light at room temperature was measured in two scattering geometries: one with the scattered light wave vectors in the YZ plane and another with the scattered light wave vectors in the YX plane. In the sample $S1$ the scattering in the YZ plane shows a strong peak at a scattering angle of 94° with respect to the Z axis, while no such peak is present around the opposite (−94°) scattering angle (Fig. 2). The polarization of the scattered light that gives this peak is orthogonal with respect to the polarization of the incident beam, i.e., it belongs to ordinary-ordinary near $Z(YX)Y$ light scattering. The ordinary-extraordinary light scattering does not show any specific maximum in the angular dependence (Fig. 3). A similar behavior was observed also for the scattering into the YX plane (Fig. 4). Here again the scattering angle of 90° corresponds to the $Z(YX)Y$ scattering. The widths of the observed peaks are instrumental and correspond to the aperture of the detecting optics used in the

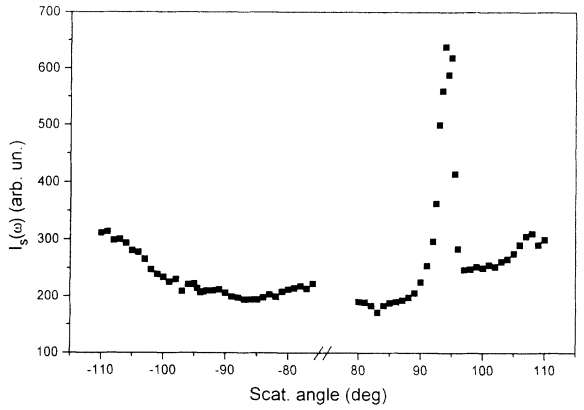

FIG. 2. Angular dependence of the intensity of the linear light scattering at room temperature. The incident light was propagating along Z axis, the scattered light was detected in the ZY plane around along Y direction (scattering angle of 90°) and around along $-Y$ direction (scattering angle of $-90°$). [For the determination of the axis with respect to the crystallographic axis and the seed plate, see Fig. 1(a).]

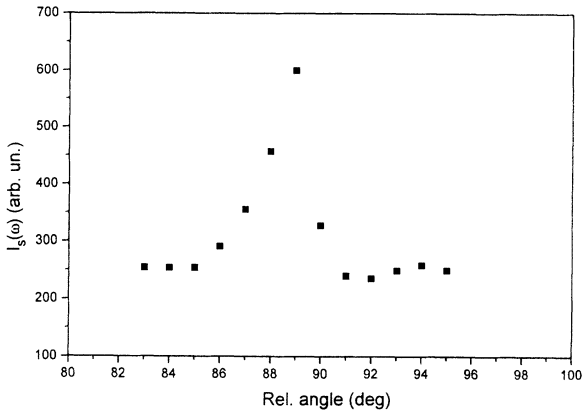

FIG. 4. Angular dependence of the ordinary-ordinary scattering for the scattering from the Z axis into the XY plane at room temperature. The relative angle of 90° corresponds to the scattering along Y axis.

actual measurement. The peak was observed only when the incident beam was propagating through the part of the sample from the pyramidal growth sector of the crystal. No peaks around 90° in the angular dependence of the linear light scattering were detected in the sample $S2$ cut out of the crystal far from the seed.

To study the temperature dependence of the intensity of the scattered radiation that corresponds to the peak in the angular dependence, the sample was mounted into a cryostate and slowly cooled (1 K/min) toward the phase transition temperature. The light polarized along the X axis and scattered into a cone of 10° around the Y axis was collected. The results are shown in Fig. 5(a). In paraelectric phase the intensity of the scattered radiation from the sample $S2$ shows almost no variation with the

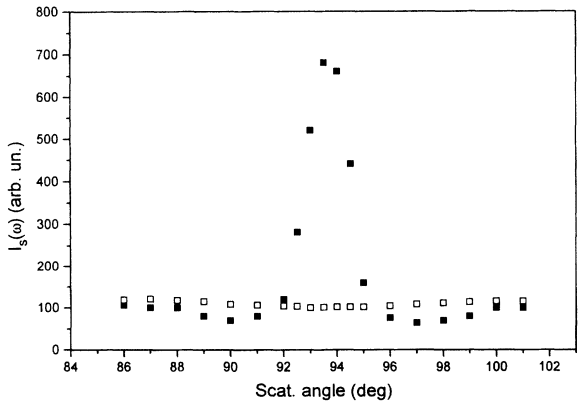

FIG. 3. Polarization dependence of the linear light scattering at room temperature. The incident light was propagating along Z axis, the scattered light was detected in the ZY plane around along Y direction. Solid squares correspond to the ordinary-ordinary scattering and empty squares to the ordinary-extraordinary scattering.

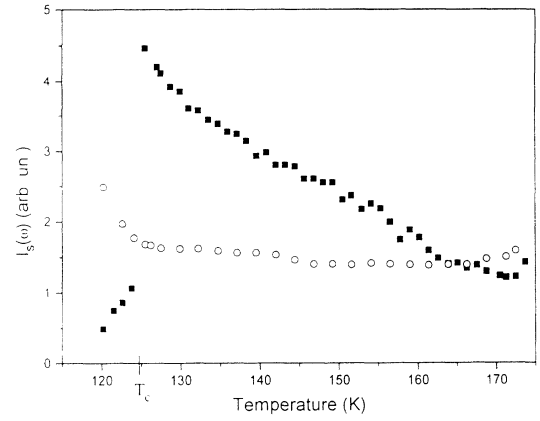

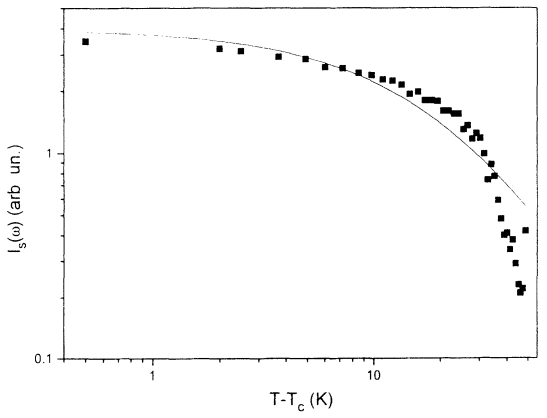

FIG. 5. (a) Temperature dependence of the linear light scattering in the scattering geometry corresponding to the peak in the angular dependence. The increase of the signal close to the transition temperature T_c corresponds to the sample $S1$ (squares), while the scattering from the sample $S2$ (circles) is almost temperature independent. (b) The fit of the data for the sample $S1$ to the theory of Levanyuk and Sigov [Eq. (5)].

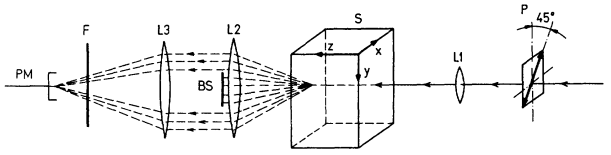

FIG. 6. Experimental setup for nonlinear light scattering: P—polarizer, $L1$—beam focusing lens, S—sample and its orientation with respect to the tetragonal axes, $L2$ and $L3$—scattered light collecting lens, BS—circular beam stop, F—filters, PM—photomultiplier. In linear light-scattering experiment in the similar geometry the incident light was polarized along Y direction and the filter in front of the photomultiplier was replaced by another polarizer.

temperature. In contrast to this the signal from the sample $S1$ starts to increase significantly ≈ 40 K above the transition temperature T_c and then continuously increases with the decreasing temperature. The signal reaches a maximum at T_c when its magnitude is about three times larger than at room temperature. Below T_c the intensity of the scattered light from both of the samples generally varies with the temperature, but the temperature dependence obtained from different measurements can be very different. This happens because the scattering in ferroelectric phase is mainly related to the presence of the ferroelectric domain walls which structure is very different from one cooling cycle to another.

For the incident beam propagating in the Z direction through the part of the sample $S1$ from the prismatic growth sector the linear light scattering at room temperature was most intense at small scattering angles. Therefore the temperature dependence of the scattered intensity was measured in the near forward scattering geometry. The unperturbed transmitted light was blocked by a circular beam stop mounted close to the light collecting lens. In this way the light scattered within the interval of scattering angles from $\vartheta = 4°$ to $\vartheta = 10°$ was detected (Fig. 6). By cooling the sample toward T_c the intensity of the scattered radiation is again increasing with decreasing temperature, but compared to the pyramidal growth sector the increase is much less significant (Fig. 7). The reason is a strong background scattering due to the reflections of the incident light from the surfaces of the sample, the sample holder, and the collimating optics. To decrease this background and increase the sensitivity of the method for the detection of lattice defects we performed a nonlinear light-scattering experiment.

B. Nonlinear scattering

In the nonlinear light-scattering experiment a beam from a Q-switched and mode-locked Nd-YAG laser ($\lambda = 1.064$ μm) with a peak power of 0.5 MW and an average power of 50 mW was used as a fundamental light source. It propagated through the sample along the Z crystallographic axis and was linearly polarized along the (110) direction. The diameter of the laser beam within the sample was around 100 μm. After passing through the sample the fundamental light was eliminated by a set of interference filters. The frequency doubled scattered radiation was detected by a photomultiplier operating in the photon counting regime. The output pulses were counted by a gated photon counter which was synchronized with the laser pulses.

For the light propagating along the Z crystallographic axis no second-harmonic generation is allowed due to the symmetry in an ideal KDP crystal either above ($\bar{4}2m$) or below ($mm2$) the transition temperature T_c. Despite this, a quite strong nonlinear signal of both orthogonal polarizations ($\|X$ and $\|Y$) was observed. The main part of the signal was associated with the coherent second-harmonic generation, which appeared to be due to the divergence ($\approx 1°$) of the incident laser beam. To eliminate this coherent part from the incoherent nonlinear scattering we again used the forward scattering geometry with the circular beam stop in front of the light collecting lens (Fig. 6).

The temperature dependence of the small angle nonlinear light scattering is shown in Fig. 8. For the sample $S1$ the intensity of the nonlinear scattered light is rela-

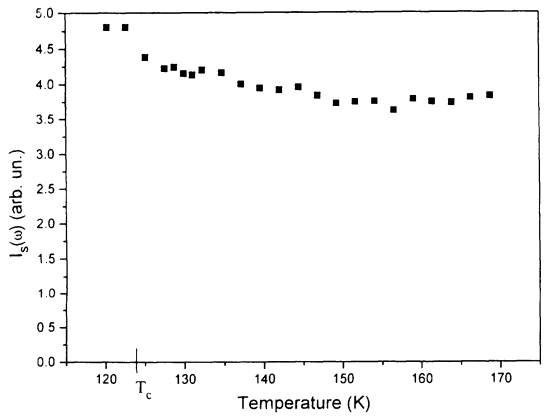

FIG. 7. Temperature dependence of the near forward scattering in the prismatic growth sector of the sample $S1$.

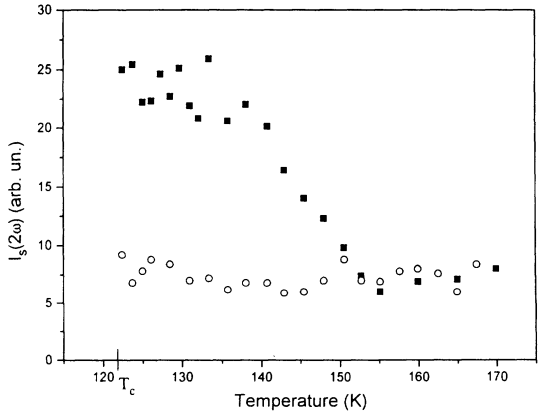

FIG. 8. Temperature dependence of the near forward second-harmonic light scattering in the prismatic growth sector of the sample $S1$ (squares) and sample $S2$ (circles).

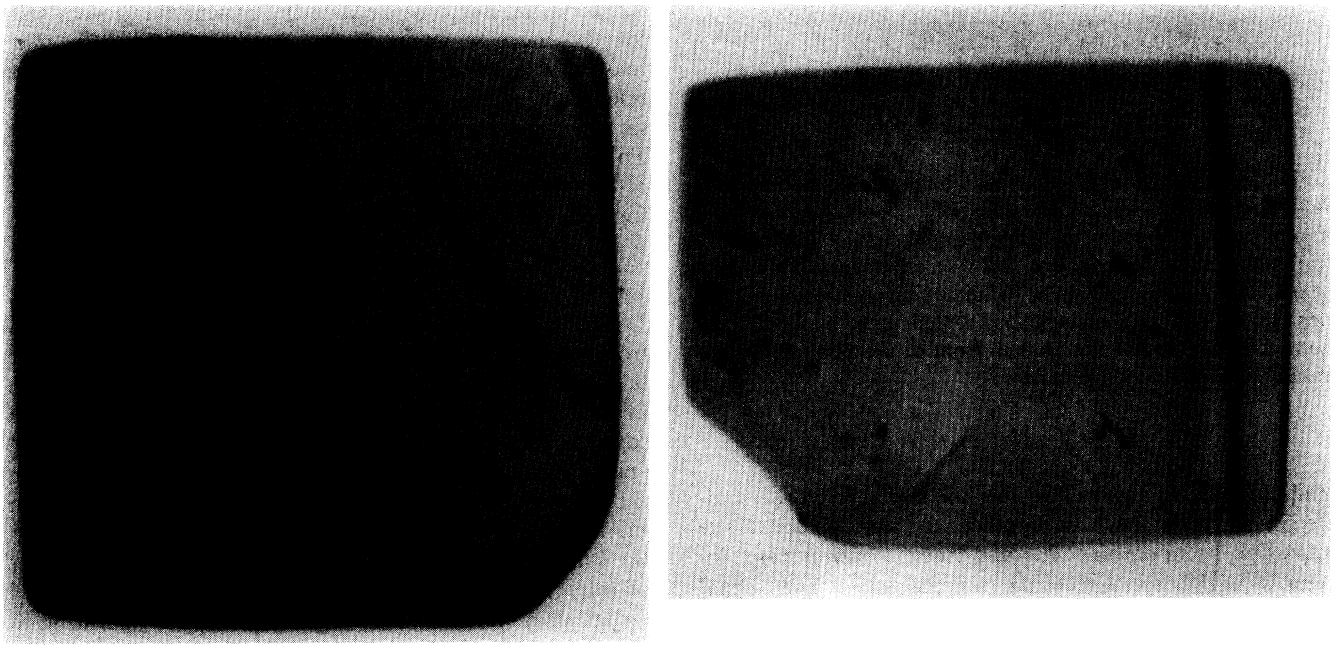

FIG. 9. X-ray topographs of the X cuts sawed from the central part of the sample $S1$ (a) and sample $S2$ (b).

tively constant at temperatures above 155 K. At 155 K it starts to increase with decreasing temperature. The increase becomes saturated ≈ 10 K above the critical temperature T_c, at a magnitude four times larger than at room temperature. For the sample $S2$ the intensity of nonlinear light scattering does not exhibit any significant temperature dependence. Below T_c the nonlinear scattering from both of the samples increases for some orders of magnitude and strongly depends on the actual ferroelectric domain structure that is formed.

C. X-ray topographic study

The structure of lattice defects in the samples $S1$ and $S2$ was investigated by Lang transmission topography using a (020) reflection of the Mo K_α radiation. Slices perpendicular to the X axis have been sawed from the central part of the samples. After polishing and etching the plates have been 0.5 mm thick. This means that we had a moderate absorption condition ($\mu d \approx 1$) for x-ray scattering.

On the topographs (Fig. 9) we can clearly recognize the growth sector boundaries (wide vertical stripes) and the dislocation lines (narrow lines). The dislocations are present only in the sample $S1$ from the zone close to the seed and most probably originate from the seed plate. Their directions correspond to the dislocations reported in the literature.[12,13] The density of any of the observed types of dislocations, which had been determined from the topographs of four slices sawed from the sample $S1$, was below 10^2 disl./cm^2. The black spots that show up particularly on the topograph of the slice from the sample $S2$ are imperfections at the surface of the slice which were caused during its preparation for the topography.

III. DISCUSSION

The most evident difference between our samples noticeable even at room temperature is a strong, almost 90° scattering, which is present only in the sample $S1$. Looking at the crystal from the "proper" direction with respect to the laser beam one can observe a bright granular speckle pattern along the path of the beam. We made several consecutive photographs of this speckle pattern [similar to photographs reported by Durvasula and Gammon for the temperatures close to T_c (Ref. 2)] which by being identical prove the static origin of this phenomenon.

Static light scattering is generally related with defects in the crystal. From the x-ray topographs of our samples the candidates for defects would be dislocations and growth sector boundaries. Starting our measurements we indeed had in mind to investigate the dislocation induced light-scattering anomalies. But we have not detected any maximum in the angular dependence of the scattering at the angles corresponding to the observed directions of the dislocation lines. On the other hand the very narrow peak in the angular dependence of the scattered light intensity at the scattering wave vector parallel to the direction of the crystal growth suggests that the scattering is related to the planar defects perpendicular to the direction of the crystal growth. This type of defects is generally called the growth bands. A similar scattering phenomenon related to planar defects has been observed in triglycine sulphate (TGS) and was associated with the planar distribution of the infinitesimal dislocation loops, which is just another name for the growth bands.[14,15]

The growth bands perpendicular to the $(0\bar{1}1)$ direction in the pyramidal growth sector and to the (010) direction

in the prismatic growth sector are clearly evident on the topograph of the crystal with a high density of the impurities [Fig. 1 (b)]. They are observed as white stripes parallel to the seed plate in the pyramidal growth sector and parallel to the XZ plane in the prismatic growth sector. The stripes correspond to the variation in the x-ray diffraction contrast due to the changes in the lattice parameters of the crystal associated with the variation in the concentration of the impurities from band to band.[16] By successive recrystallizations the average concentration of the impurities decreases and the diffraction contrast of the bands becomes too low to be visible on the topographs. But the bands might still have a strong effect on the light scattering. The appearance of the growth bands in KDP is mostly restricted to the zone close to the seed where they are in strong correlation with the numerous dislocations originating from the seed plate.[17] Considering this correlation we conclude that in our case the bands were much more pronounced in the sample $S1$ than in the sample $S2$.

A. Linear scattering

Although in our experiment intensity of the scattered radiation was measured in a broad spectral band, the main part of the signal corresponds to elastic light scattering. The intensity of the linearly scattered light $I_s(\omega)$ is proportional to the square of the scattered field

$$E_s(\omega,\mathbf{k}_s)\propto\int \mathbf{v}_s\chi^{(1)}(\mathbf{r})\mathbf{v}_i e^{i(\mathbf{k}_i-\mathbf{k}_s)\mathbf{r}}dV\ , \tag{1}$$

where $\chi^{(1)}$ is the linear dielectric susceptibility tensor at incident optical frequency and $\mathbf{k}_i$, $\mathbf{v}_i$, $\mathbf{k}_s$, and $\mathbf{v}_s$ are the wave vectors and the polarization vectors of the incident and scattered light. The spatial dependence of $\chi^{(1)}$ is related with the spatial variation of the concentration of the impurities and the strain field decorating impurities. For the most simple case of impurity induced nonpolar point defects it is given by

$$\chi^{(1)}_{si}(\mathbf{r})\doteq\tilde{\chi}_{si}-\tilde{\chi}_{ss}\tilde{\chi}_{ii}p_{sijk}\int S_{jk}(\mathbf{r}-\mathbf{r}')\rho(\mathbf{r}')dV'\ , \tag{2}$$

where $\tilde{\chi}$ is the susceptibility tensor of the nonstrained crystal, ρ is the density of the impurities, S is the strain field of a single defect, and p is the first order elasto-optic (Pockel's) tensor. The scattered field is then

$$E_s(\omega,\mathbf{k}_s)\propto v_s v_i p_{sijk}S_{jk}(\mathbf{q})\rho(\mathbf{q})\ , \tag{3}$$

where $S_{jk}(\mathbf{q})$ and $\rho(\mathbf{q})$ are the spatial Fourier components of the strain field and impurity density at the scattering wave vector $\mathbf{q}=(\mathbf{k}_i-\mathbf{k}_s)$.

For the impurity concentration changing in well defined planar bands

$$\rho(\mathbf{q})\approx\delta(\mathbf{s}_q-\mathbf{s}_o)\rho_o\ , \tag{4}$$

where $\mathbf{s}_q=\mathbf{q}/q$ and $\mathbf{s}_o$ is a band's normal, the last term in relation (3) plays the leading role in the angular dependence of the light scattering and results in a narrow peak for scattering wave vector along $\mathbf{s}_o$. The planes of impurities thus give a specular reflection. The temperature dependence of the scattering is governed mostly by the strain dependent term in (3). The critical strain corresponding to the soft acoustic mode in KDP is the S_{xy} shear, which is coupled to the χ_{xy} component of the linear dielectric susceptibility. In the crystal containing defects χ_{xy} will thus strongly increase as the critical temperature is approached from above whereas the other components will change only very little. The observed polarization dependence of the scattered light at room temperature shows that the χ_{xy} component of the susceptibility is most strongly affected by defects also at high temperatures. This is the consequence of the strong anisotropy of the elasto-optic and elastic properties of the crystal.

The temperature and spatial dependence of the critical S_{xy} strain in the vicinity of a point defect in KDP has been extensively studied by Levanyuk and Sigov (Ref. 8, p. 117). They used the Landau-Ginzburg theory of phase transitions to calculate the strain field of an isolated charged defect and an unpolar s defect. For the experimental geometry used in the pyramidal growth sector part of the sample with the scattering wave vector $\mathbf{q}$ along the $(0\bar{1}1)$ crystallographic direction their calculations give

$$I_s(\omega,T)\propto\left[(T-T_c)+\frac{C/\epsilon_a}{(c/a)^2+1}\right]^{-2}\ . \tag{5}$$

Taking the values for the lattice constants a and c, the Curie constant C and the dielectric constant ϵ_a from Ref. 18, the second term on the right-hand side of (5) is 31 K. In the interval between T_c and T_c+31 K a considerable deviation from the usual $(T-T_c)^{-2}$ dependence is expected. Comparing this result with our experimental data one can notice that the temperature dependence of the scattered light intensity indeed starts to deviate from the power law at approximately 30 K above the transition temperature T_c that is in good agreement with the theory [Fig. 5(b)]. But on the other hand the discrepancy with the overall theoretical curve is quite large. It might be related to the inaccuracy in the determination of the background scattering, which we took to be the room temperature value of the scattered intensity. The other reason for the discrepancy in the temperature behavior might be an overlapping of the strain fields of the impurities, which is not taken into account in Eq. (5). This possibility will be discussed in more detail for the case of nonlinear scattering.

B. Nonlinear scattering

The main contribution to the observed second-harmonic signal originates from the inhomogenity of the nonlinear susceptibility tensor $\chi^{(2)}(\mathbf{r})$. The scattered field radiated by the induced nonlinear polarization is then

$$E_s(2\omega,\mathbf{k}_s)\propto\int\chi^{(2)}(\mathbf{r}):\mathbf{v}_s\mathbf{v}_i\mathbf{v}_i e^{i(2\mathbf{k}_i-\mathbf{k}_s)\mathbf{r}}dV\ , \tag{6}$$

where $\mathbf{k}_i$, $\mathbf{v}_i$, $\mathbf{k}_s$, and $\mathbf{v}_s$ again denote the wave vectors and the polarization vectors of the incident and scattered light. The scattering wave vector $\mathbf{q}$ is in this case defined as $(2\mathbf{k}_i-\mathbf{k}_s)$. The spatial dependence of the nonlinear

susceptibility expressed in relation to the strain field is

$$\chi^{(2)}_{sij}(\mathbf{r}) \doteq \tilde{\chi}_{sij} + b_{sijkl} \int S_{kl}(\mathbf{r}-\mathbf{r}')\rho(\mathbf{r}')dV' \ , \tag{7}$$

where b is a second order elasto-optic tensor. The critical S_{xy} strain is here coupled to three components of $\chi^{(2)}$. These are χ_{xxz}, χ_{yyz}, and χ_{zzz}, which are all zero in the ideal nonstrained crystal. In the strained crystal they will have nonzero values and will show a strong temperature dependence.

Following the previous discussion on the angular dependence of the linear scattering, which is valid also for nonlinear scattering, the experimental geometry with the incident beam along the Z crystallographic axis is not very efficient for the study of growth bands normal to the (010) direction. But as the area of the prismatic growth sector in our samples was relatively narrow this was the only appropriate geometry. For this geometry the calculations of Levanyuk and Sigov[8] result in

$$I_s(2\omega, T) \propto \left[(T-T_c) + \frac{C/\epsilon_a}{[n_{2\omega}\vartheta/(n_{2\omega}-n_\omega)]^2+1} \right]^{-2} , \tag{8}$$

where ϑ is the scattering angle and n_ω and $n_{2\omega}$ are the ordinary refractive indices of the incident and second harmonic beam. In the interval of scattering angles covered by our experiment (from $\vartheta=4°$ to $\vartheta=10°$) the second term on the right-hand side of (8) is between 2 and 0.35 K. The nonlinear scattering for isolated defects is thus expected to exhibit a $(T-T_c)^{-2}$ power law temperature dependence at all the temperatures except very close to T_c. In our experiment, however, a significant saturation of the scattering was observed already at 15 K above T_c (Fig. 8). For that reason we suggest that the deviation from the power law is a consequence of the overlap of the deformed regions of single defects, which starts around this temperature.

The characteristic dimension r_c of the strained regions decorating the impurities is critically increasing in the vicinity of T_c. At a temperature corresponding to the condition $\rho r_c^3 = 1$ the deformed regions of the neighboring impurities start to overlap and a further increase of the overall strain is suppressed. This changes the temperature behavior of the light scattering.[19] The average density of the impurities in our crystal as determined by neutron activation analysis was 3×10^{17} cm^{-3}. This results in an interimpurity distance of 15 nm. But as most of the impurities segregate in the zone close to the seed the interimpurity distance in the sample $S1$ was a few times lower. From our measurements we conclude that at 15 K above the transition temperature T_c the influence radius r_c of the impurities increases to the value of around 5 nm. Unfortunately we do not know of any neutron scattering investigation of the temperature dependence of r_c to verify this result.

We may thus conclude that the observed strong angular and temperature anomalies of the linear as well as nonlinear elastic light scattering in KDP are the result of the growth bands which form a set of planes with different concentration of the impurities. The orientation and the expressiveness of the bands is determined by the growth process. The unusual saturation behavior pronounced in the temperature dependence of the nonlinear scattering is explained with the overlap of the deformed regions decorating the impurities. Further systematic investigations of the light scattering on the crystals with different concentration of the impurities are necessary to obtain a quantitative description of this saturation behavior.

ACKNOWLEDGMENTS

One of the authors, I.D., is grateful to the Austrian Bundesministerium fuer Wissenschaft und Forschung (GZ 45.223/2-27b/91) for supporting her stay at the Institut fuer Experimentalphysik der Universitaet Wien.

*Present address: Institute of Quantum Electronics, Swiss Federal Institute of Technology, CH-8093 Zurich, Switzerland.

[1]N. C. Lagakos and H. Z. Cummins, Phys. Rev. **B10**, 1063 (1974).
[2]L. N. Durvasula and R. W. Gammon, Phys. Rev. Lett. **38**, 1081 (1977).
[3]E. Courtens, Phys. Rev. Lett. **39**, 561 (1977); **41**, 1171 (1978).
[4]E. Courtens and R. Gammon, Ferroelectrics **24**, 19 (1980).
[5]E. Courtens, Phys. Rev. B **24**, 3890 (1981).
[6]R. Blinc, J. Slak, F. C. SaBarreto, and A. S. T. Pires, Phys. Rev. Lett. **42**, 1000 (1979).
[7]A. S. Chaves and R. Blinc, Phys. Rev. Lett. **43**, 1037 (1979).
[8]A. P. Levanyuk and A. S. Sigov, *Defects and Structural Phase Transitions* (Gordon and Breach, New York, 1987).
[9]A. A. Isaverdiev, Yu. M. Kishinetz, A. P. Levanyuk, A. I. Morosov, and A. S. Sigov, Ferroelectrics **106**, 3 (1990).
[10]E. Sandvold, T. Laegreid, K. Fossheim, and J. O. Fossum, Phase Transitions, **11**, 145 (1988).
[11]A. Fuith, T. Streuselberger, and H. Warhanek, J. Cryst. Growth, **97**, 469 (1989).
[12]H. Newkirk, J. Swain, S. Stokowski, D. Milam, D. Smith, and H. Klapper, J. Cryst. Growth, **65**, 651 (1983).
[13]H. Klapper, Yu. M. Fishman, V. G. Lutsau, Phys. Status Solidi A **21**, 115 (1974).
[14]A. Fouskova, M. Pavel, and B. Brezina, Phys. Status Solidi A **81**, K117 (1984).
[15]L. Lejček, A. Fouskova, and M. Pavel, Phys. Status Solidi A **115**, 445 (1989).
[16]See, for instance, B. Dam and W. J. P. Van Enckevort, J. Cryst. Growth **51**, 607 (1981), and the references cited therein.
[17]C. Belouet, E. Dunia, and J. F. Petroff, J. Cryst. Growth **23**, 243 (1974).
[18]*Numerical Data and Functional Relationships in Science and Technology,* Landolt-Bornstein, New Series Vol. 16, Ferroelectrics and Related Substances, edited by K. H. Hellwege and A. M. Hellwege (Springer-Verlag, Berlin, 1982).
[19]N. I. Lebedev, A. P. Levanyuk, A. I. Morozov, and A. S. Sigov, Fiz. Tverd. Tela (Leningrad) **25**, 2979 (1983) [Sov. Phys. Solid State **25**, 1719 (1983)].

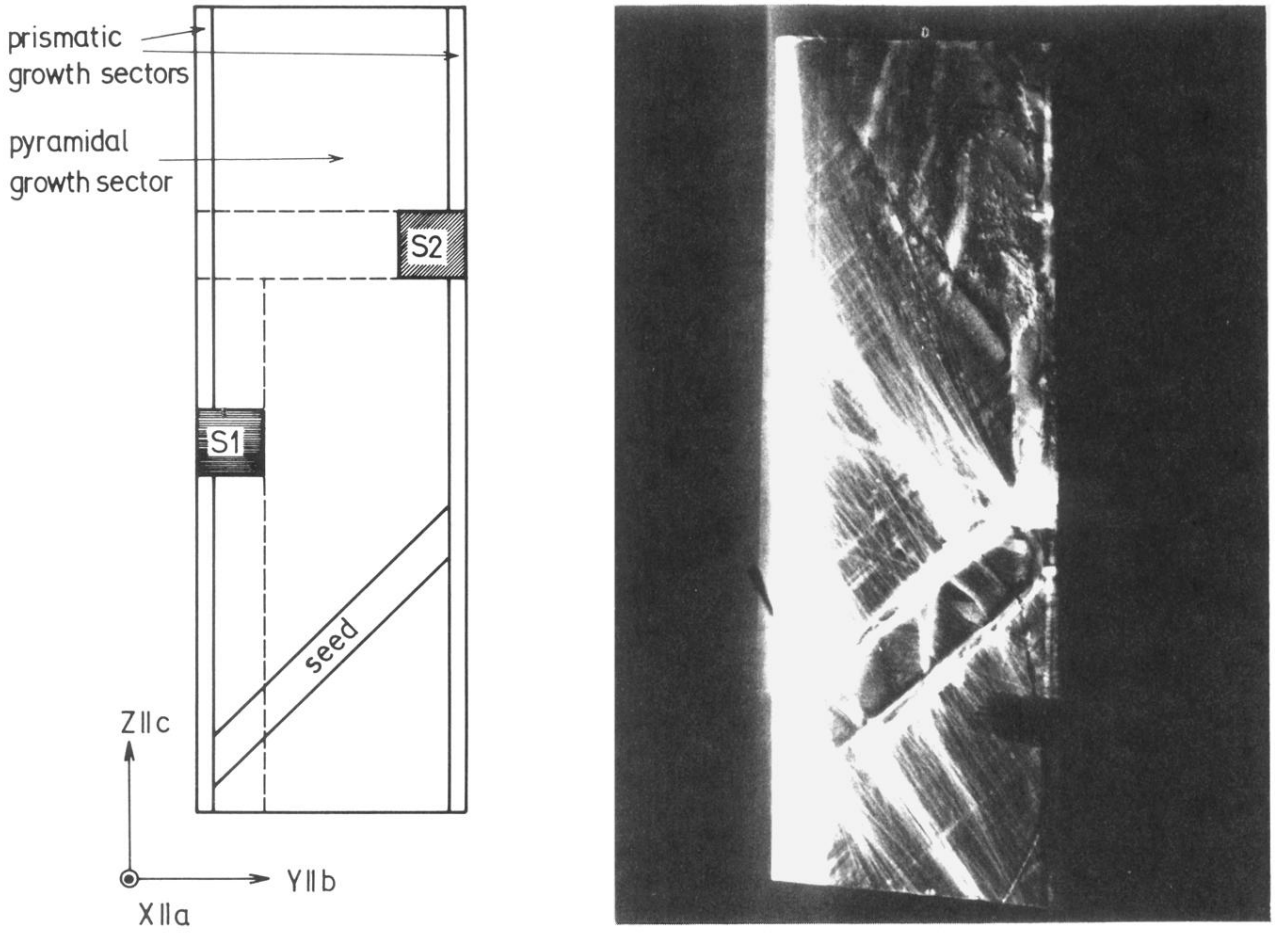

FIG. 1. (a) Schematic drawing of an X cut of the crystal, showing the regions which were sawed for the samples $S1$ and $S2$. (b) X-ray topograph of an X cut of the crystal with high density (15 000 ppm) of impurities.

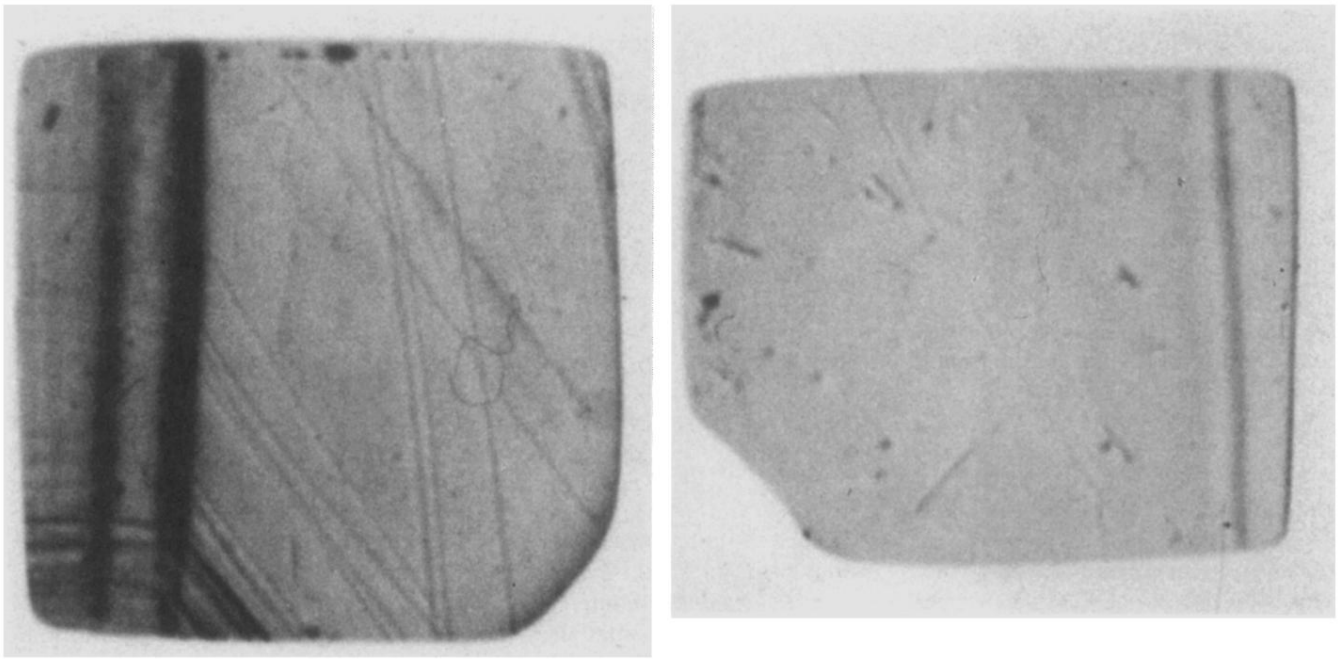

FIG. 9. X-ray topographs of the X cuts sawed from the central part of the sample $S1$ (a) and sample $S2$ (b).